One- and two-photon detachment of O^-

Matthieu Génévriez,[1,*] Xavier Urbain,[1] Arnaud Dochain,[1] Alain Cyr,[2,3] Kevin M. Dunseath,[2] and Mariko Terao-Dunseath[2]
[1]*Institute of Condensed Matter and Nanosciences, Université Catholique de Louvain, Louvain-la-Neuve B-1348, Belgium*
[2]*Institut de Physique de Rennes, UMR 6251 CNRS–Université de Rennes 1, Campus de Beaulieu, F-35042 Rennes cedex, France*
[3]*IBM Client Center, 34006 Montpellier, France*
(Received 27 May 2016; published 10 August 2016)

Cross sections for one- and two-photon detachment of $O^-(1s^2 2s^2 2p^5\ ^2P^o)$ have been determined in a joint experimental and theoretical study. The absolute measurement is based on the animated-crossed-beam technique, which is extended to the case of pulsed lasers, pulsed ion beams, and multiphoton detachment. The *ab initio* calculations employ *R*-matrix Floquet theory, with simple descriptions of the initial bound state and the residual oxygen atom which reproduce well the electron affinity and ground-state polarizability. For one-photon detachment, the measured and computed cross sections are in good mutual agreement, departing significantly from previous reference experiments and calculations. The generalized two-photon detachment cross section, measured at the Nd:YAG laser wavelength, is in good agreement with the *R*-matrix Floquet calculations. Long-standing discrepancies between theory and experiment are thus resolved.

DOI: 10.1103/PhysRevA.94.023407

I. INTRODUCTION

The one-photon detachment of the oxygen negative ion $O^-(1s^2 2s^2 2p^5\ ^2P^o)$ was first investigated some 60 years ago by Branscomb and Smith [1] and then by Branscomb *et al.* [2]. A third, absolute measurement by Smith [3] provided slightly different cross sections, while the relative measurement of Branscomb *et al.* [4] extended the photon energy range. Two later independent absolute measurements [5,6], albeit over a limited energy range, confirmed the values of [3,4]. These were thus considered as a reference and have since been used to normalize relative photodetachment cross sections for other ions such as C^-, B^-, O_2^- [7–10]. The determination of photodetachment cross sections for the open-shell O^- ion remains a challenging task for theories, as electron correlations and polarization effects play an important role. A number of attempts over the last few decades (see [11] and references therein) yielded results that vary widely and do not match the experimental data, neither in magnitude nor in shape. The values of the latest and most extensive calculation [11] lie significantly higher than those of [3,4]. The pronounced disagreement between theory and experiment and the use of the latter for normalizing other quantities calls for further investigation.

The two-photon detachment of O^- has not been widely studied and the agreement between the few results available is not particularly good. The only existing experiment gives a generalized cross section of $(4.2^{+1.9}_{-1.6}) \times 10^{-50}$ cm^4 s at a wavelength of 1064 nm [12]. An early calculation based on perturbation theory and a one-electron model potential [13] yields, after interpolation, a value of 1.8×10^{-49} cm^4 s, which is more than four times larger. The results obtained using an adiabatic theory [14] are almost an order of magnitude larger than experiment. Clearly, there is room for improvement.

Here, we report the results of a new absolute measurement of the one-photon and generalized two-photon detachment cross sections. The measurement was performed using the animated-crossed-beam technique which does not require assumptions about the profiles of the laser and ion beams, and which has been successfully applied to the photodetachment of H^- [15]. The technique is extended to the two-photon case, at the price of a few additional, reasonable assumptions. We have also performed a series of calculations for the one-photon and generalized two-photon detachment cross section using the *R*-matrix Floquet method [16,17]. Standard *R*-matrix [18] calculations were also performed for the one-photon case. As we shall show below, the new theoretical and experimental values are in good agreement, and depart from the commonly admitted values.

II. EXPERIMENT

The experimental setup, sketched in Fig. 1, is essentially the same as that used by Génévriez and Urbain [15]. The oxygen anions are produced by a duoplasmatron source fed with N_2O gas and accelerated to 4 or 6 keV. The anion beam is directed towards the interaction region by a set of planar deflectors. Its direction x in the interaction region is defined by a circular diaphragm (D_1, radius 1 mm) and a rectangular diaphragm (D_2, 1 mm along z, 100 μm along y). These are carefully aligned with the apertures of the quadrupolar deflector Q and the detector located downstream to ensure the detection of all the oxygen atoms produced by the laser. The second diaphragm is a slit whose width is of the order of the spot size of the focused laser beam, strongly reducing the background signal from sections of the ion beam where the light intensity is negligible.

Different lasers have been used in order to cover a wide range of wavelengths. For one-photon detachment between 700 and 845 nm, we used a CW Ti:sapphire laser (3900S, Spectra Physics) pumped by an Ar^+ laser (Innova 400, Coherent). The lines from the same Ar^+ laser cover the range from 457.9 to 514.5 nm. A DPSS laser (Verdi-V10, Coherent) provides light at a wavelength of 532 nm and a diode laser (CNI, MDL-III-405) at 405 nm. The laser

*matthieu.genevriez@uclouvain.be

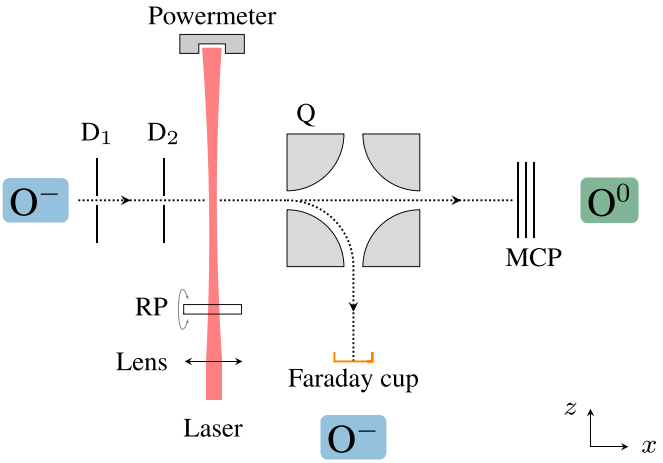

FIG. 1. Experimental setup. D_1: circular diaphragm, D_2: rectangular diaphragm, RP: rotating glass plate, Q: quadrupolar deflector, MCP: multichannel plates.

power in the interaction region ranges from 60 mW to a few hundred mW.

Two-photon experiments require higher intensities, only attainable with pulsed lasers, and are limited to below the one-photon threshold (848.6 nm). We used a Q-switched Nd:YAG laser (Precision II 9030, Continuum) providing nanosecond pulses with an initial energy of about 500 mJ, which is reduced to a few mJ by the combination of three methods: (i) varying the delay between the optical pumping of the Nd:YAG rod and the opening of the Q switch; (ii) selecting the reflection of the beam on a bare glass plate; (iii) combining a $\lambda/2$ plate and a polarizing beam splitter.

The pulsed Nd:YAG laser is inherently a multimode laser, producing chaotic light which can affect the measurement of multiphoton cross sections [19–21]. To assess the importance of this in our experiment, we also operated the laser with a single mode by injecting the light of a seeding laser (temperature-controlled laser diode) into the cavity. The time envelope of the output pulse was monitored with a fast photodiode, and deviation from the single-mode regime due to temperature variations of the diode clearly appeared as intensity beatings. The fast photodiode has a rise time of 1 ns, according to the manufacturer.

The laser beam is focused onto the O^- beam by an $f = 40$ cm lens. It then passes through a glass plate mounted on a high-accuracy rotation stage. By tilting the plate around the x axis, the laser beam can be vertically displaced, or "animated," at will. The relation between the tilt angle and the vertical displacement follows from the Snell-Descartes law, and has been checked against direct measurements [15]. Finally, the light enters and leaves the interaction chamber through laser windows with antireflection coating. It is then collected on a power meter for the CW lasers, or a pyroelectric energy meter for the pulsed laser. The power meter has an accuracy of 3% and has been recalibrated by the manufacturer prior to the measurement. The energy meter has an accuracy of 5%. We checked that the reflectivity and absorbance of the windows have a negligible impact on the power or energy of the laser beam, as expected from the manufacturer's specifications.

After the interaction region, a quadrupole deflects the remaining negative ions into a Faraday cup, while the neutral oxygen atoms pass straight through and are collected by either a channel electron multiplier (CEM) for one-photon detachment or multichannel plates (MCP) for two-photon detachment. In the one-photon experiment, detection is identical to that previously described [15]. For two-photon detachment, the neutrals are counted during a narrow time window (∼20 ns) delayed with respect to the laser shot by the neutrals' time of flight (∼ 2.3 μs). The background mainly arises from collisional detachment with the residual gas and is of the order of 13 kHz for an ion beam current of ∼100 pA. The detection of neutral atoms produced by photodetachment is thus essentially background free due to the brevity of the inspection window. The detection efficiency of the MCP, 56%, is estimated by comparing its count rate with that of a CEM whose efficiency is known [22].

III. ANIMATED CROSSED BEAMS

Absolute cross sections are notoriously difficult to measure due to the necessity of accurately determining the interaction volume. The problem is frequently overcome by assuming reasonable shapes for the interacting beams. However, any departure from these ideal shapes introduces discrepancies between data. A much more efficient method consists in scanning the profile of one of the beams with the other, the so-called animated-crossed-beam technique (ACBT) first proposed by Brouillard and Defrance [23,24] for electron-ion collisions and subsequently applied to one-photon light-matter interactions [15,25]. It is readily shown that the absolute cross section depends only on experimental parameters that are easy to determine accurately, with very few assumptions made concerning the shape of the interacting beams. The method relies on sweeping the laser beam along the y axis, i.e., perpendicularly to the interaction plane (see Fig. 1), and on measuring the rate $R(Y)$ at which neutral atoms are produced, where Y is the position of the center of the laser beam. The laser power P_{laser} and the ion current I_{ion} are continuously recorded and used to normalize the corresponding value of $R(Y)$. The cross section $\sigma^{(1)}$ is then given by

$$\sigma^{(1)} \simeq \frac{\mathrm{e}\, v}{\eta}\left[\int dY\, R(Y)\right]\frac{\hbar\omega}{I_{\text{ion}}\, P_{\text{laser}}}, \tag{1}$$

where v is the speed of the ions, η is the detection efficiency, $\hbar\omega$ is the photon energy, and e is the elementary charge. Expression (1) is valid for all processes that depend linearly on the incoming flux of particles, be it ions, photons, or electrons. In the one-photon experiment, the laser power must therefore be kept low enough to avoid saturation of the photodetachment process.

A. Multiphoton extension

It is easy to see why the standard ACBT does not apply to multiphoton processes. In such cases, the detachment rate p is the product of the generalized n-photon detachment cross section $\sigma^{(n)}$ with the nth power of the photon flux Φ:

$$p(x,y,z,\tau) = \sigma^{(n)}\Phi^n\left(x,y,z,\tau+\frac{x}{v}\right), \tag{2}$$

where the coordinates (x,y,z) are as defined in Fig. 1 and the time $\tau = 0$ corresponds to the maximum of the laser pulse envelope. The final detachment probability $P(y,z,\tau)$, after the ion has traveled through the laser spot, is given by

$$P(y,z,\tau) = 1 - \exp\left[-\frac{1}{v}\int_{-\infty}^{+\infty} dx\; p(x,y,z,\tau)\right]. \quad (3)$$

As for the one-photon ACBT, we assume that the photon flux is sufficiently low for n-photon detachment to occur in the perturbative regime. Expanding the exponential and retaining the first-order term gives

$$P(y,z,\tau) \simeq \frac{\sigma^{(n)}}{v}\int_{-\infty}^{+\infty} dx\; \Phi^n\left(x,y,z,\tau + \frac{x}{v}\right). \quad (4)$$

For each vertical offset Y of the center of the laser beam with respect to the center of the O^- beam, the yield $N(Y)$ of neutrals is given by integrating the n-photon detachment probability P over all positions (y,z) within the section S of the ion beam and over the traversal time τ through the laser pulse:

$$N(Y) = \frac{\eta\sigma^{(n)}}{\mathrm{e}\,v}\iint_S dy\,dz\; j(y,z) \times \int d\tau \int_{-\infty}^{+\infty} dx\; \Phi^n\left(x,y-Y,z,\tau + \frac{x}{v}\right), \quad (5)$$

where $j(y,z)$ is the local current density of O^-. By integrating both sides of (5) over Y, we obtain an expression for the generalized n-photon detachment cross section:

$$\sigma^{(n)} = \frac{\mathrm{e}\,v}{\eta}\left[\int dY\; N(Y)\right]\left[\iint_S dy\,dz\; j(y,z) \times \iiint_{-\infty}^{+\infty} d\tau\,dY\,dx\; \Phi^n\left(x,y-Y,z,\tau+\frac{x}{v}\right)\right]^{-1}. \quad (6)$$

For one-photon processes ($n = 1$), the integral of Φ over τ, Y, and x reduces to the number of photons per pulse $E_{\mathrm{laser}}/\hbar\omega$, where E_{laser} is the laser pulse energy. The integral of $j(y,z)$ over y and z then reduces to the ion current I_{ion}. Equation (6) thus generalizes Eq. (1) to the case of pulsed lasers:

$$\sigma^{(1)} = \frac{\mathrm{e}\,v}{\eta}\left[\int dY\; N(Y)\right]\frac{\hbar\omega}{I_{\mathrm{ion}}E_{\mathrm{laser}}}. \quad (7)$$

In the multiphoton case ($n \geqslant 2$), the integral of Φ^n over τ, Y, and x appearing in Eq. (6) does not reduce to the number of photons per pulse and the cross section cannot be recovered as straightforwardly as in the standard ACBT. In the next section, we present two alternative methods for expressing the cross section in terms of accurately measurable quantities by introducing a small set of reasonable assumptions.

First, the confocal parameter of the laser beam is about 2 cm, 20 times larger than the width of the ion beam along the z axis. Therefore, the variations of the photon flux along z are negligible in the region where photodetachment occurs. Second, it is reasonable to assume that $\Phi(x,y,z,\tau)$ can be factorized into a temporal envelope $g(\tau)$ and a spatial profile $\phi(x,y)$ which, as just explained, does not depend on z. Finally, we define $\rho_y(y)$ as the normalized projection of the current density $j(y,z)$ onto the y axis,

$$\int dz\; j(y,z) = I_{\mathrm{ion}}\,\rho_y(y), \quad (8)$$

where I_{ion} is the ion beam current.

With the above assumptions, Eq. (5) for the yield $N(Y)$ can be written as

$$N(Y) = \frac{\eta\sigma^{(n)}}{\mathrm{e}\,v}\Delta^{(n)} I_{\mathrm{ion}} \times \int dy\;\rho_y(y)\int_{-\infty}^{\infty} dx\;\phi^n(x,y-Y), \quad (9)$$

where $\Delta^{(n)}$ is the integral of the nth power of the time profile of the laser pulse

$$\Delta^{(n)} = \int_{-\infty}^{+\infty} d\tau\; g^n(\tau + x/v) = \int_{-\infty}^{+\infty} d\tau\; g^n(\tau). \quad (10)$$

Note that the above equations are valid for continuous ion beams. Similar equations can be obtained in the case of pulsed ion beams, as shown in the Appendix A.

B. Generalized two-photon cross sections

We present two alternative methods for expressing the generalized two-photon cross section [$n = 2$ in Eq. (9)] in terms of precisely measurable quantities. The generalization of these methods to higher numbers of photons ($n \geqslant 3$) is straightforward.

The first and simplest approach is to approximate the spatial distribution of the photon flux by a Gaussian,

$$\phi(x,y) = \frac{1}{\hbar\omega}\frac{2E_{\mathrm{laser}}}{\pi w_0^2\Delta}e^{-2(x^2+y^2)/w_0^2}, \quad (11)$$

where w_0 is the laser waist and $\Delta = \int d\tau\; g(\tau)$. The choice of a Gaussian distribution is justified by the fact that our pulsed laser operates near the TEM00 mode. The integral of the square of the photon flux can now be evaluated analytically and the generalized two-photon cross section is thus given by

$$\sigma^{(2)} = \frac{\mathrm{e}v}{\eta I_{\mathrm{ion}}}\left(\frac{\hbar\omega}{E_{\mathrm{laser}}}\right)^2\frac{\Delta^2}{\Delta^{(2)}}\pi w_0^2\int N(Y)dY. \quad (12)$$

Note that we have made no assumptions about the shape of the ion beam.

The second method for expressing the integral of ϕ^2, present in Eq. (9), in terms of easily measurable quantities and without modeling the shape of the laser beam, exploits the fact that the transit of the ions through the laser focus amounts to a tomography of the intensity profile, as shown in Fig. 2.

Let us first define a succession $\mathcal{A}$ of integral transforms, which transforms a function $f(x,y)$ into a function $F(Y)$ as follows:

$$F(Y) = \mathcal{A}[f(x,y)] = \int dy\;\rho_y(y)\int_{-\infty}^{+\infty} dx\; f(x,y-Y). \quad (13)$$

Equation (9) with $n = 2$ can then be rewritten as

$$N(Y) = \frac{\eta\sigma^{(2)}}{\mathrm{e}\,v}\Delta^{(2)} I_{\mathrm{ion}}\,\mathcal{A}[\phi^2(x,y)]. \quad (14)$$

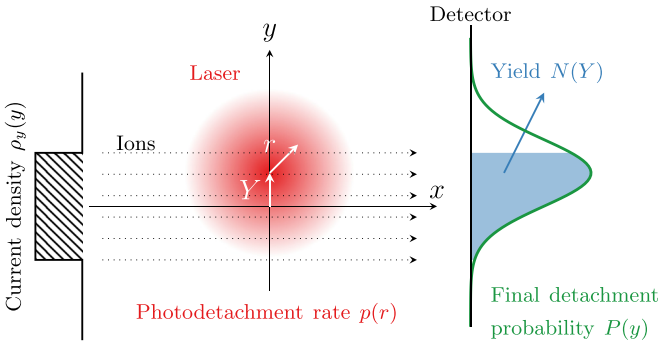

FIG. 2. Idealized representation of the experiment. The detachment rate, proportional to the square of the photon flux, is integrated along the ion trajectory (dotted lines) to obtain the final detachment probability (thick curve), as in (4). The latter is subsequently convolved with the normalized projection ρ_y of the current density onto the y axis (hatched area) to obtain the yield N (shaded area) defined in (5).

It is reasonable to assume that ϕ is symmetric under rotation around the light propagation axis z as our laser operates near the TEM00 mode. The integral over the line of sight x can then be interpreted as the Abel transform of the detachment probability $p = \sigma^{(2)}\phi^2$ [26]. The standard definition of the transform appears immediately when rewriting the integral in cylindrical coordinates

$$N(Y) = \frac{2\eta}{\mathrm{e}\, v}\Delta^{(2)} I_{\mathrm{ion}} \int dy \rho_y(y) \int_{y-Y}^{+\infty} dr \frac{r p(r)}{\sqrt{r^2-(y-Y)^2}}. \tag{15}$$

The path integral of an atom traveling in a straight line through the laser spot corresponds to the Abel transform $P(y-Y)$ of the detachment rate $p(r)$ at a vertical position $y-Y$. The convolution with the normalized current density $\rho_y(y)$ in the second integral subsequently "blurs" the transform $P(y-Y)$, similar to the point-spread function of an imaging device [27]. It is possible to recover $p(r)$ from the measured yield $N(Y)$ by numerically inverting the two integral transforms using one of the techniques from the extensive range available [28].

The comparison of ρ_y with a point-spread function highlights the importance of the respective sizes of the ion and laser beams. If the laser beam is much narrower than the ion beam, the blurring effect becomes too strong to recover the final detachment probability. The radius of the ion beam along the vertical direction must be kept of the order of or smaller than the waist of the laser beam. To do so, an aperture 100 μm in height was used to define the ion beam, matching the $\sim$120 μm diameter of the laser spot.

Although an analytical formula can be obtained for inverting $\mathcal{A}$, it is in practice cumbersome and involves derivatives of the measured signal. A more efficient method for performing the Abel inversion consists in expanding the measured yield in a basis of functions ψ_m spanning the "detection" space

$$N(Y) = \sum_{m=1}^{m_{\max}} c_m \psi_m(Y), \tag{16}$$

and the detachment rate in a basis of functions φ_m spanning the "detachment" space

$$p(r) = A \sum_{m=1}^{m_{\max}} c_m \varphi_m(r), \tag{17}$$

where A is a constant. The two basis sets are related through

$$\psi_m(Y) = 2 \int dy\, \rho_y(y) \int_{y-Y}^{+\infty} dr \frac{r\varphi_m(r)}{\sqrt{r^2-(y-Y)^2}}. \tag{18}$$

Comparing Eqs. (18) and (15) gives

$$A = \frac{\mathrm{e}\, v}{\eta \Delta^{(2)} I_{\mathrm{ion}}}. \tag{19}$$

Since the pulsed laser used for this study operates near the TEM00 mode, a basis of Gaussian functions with varying widths is appropriate:

$$\varphi_m(r) = e^{-r^2/[a+(m-1)b]^2}. \tag{20}$$

The parameters a and b and the number $m_{\max}$ of functions define the interval spanned by the widths of the functions and their density. They are chosen so that the estimated width of the laser beam lies close to the center of this interval and that the upper and lower limits lie sufficiently far away.

The functions ψ_m are then computed from φ_m using (18). The Abel transform of a Gaussian function is another Gaussian function [26]. If ρ_y is analytical and well behaved, the convolution by ρ_y can be derived analytically, otherwise it must be performed numerically. This is, for example, the case when ρ_y is provided as a set of experimental data. The ion beam in the experiment is well collimated so that we can assume that ρ_y is a uniform distribution. Therefore, the basis functions ψ_m can be expressed as the difference of two error functions

$$\psi_m(Y) = \frac{\pi w_m^2}{2L}\left[\mathrm{erf}\left(\frac{Y+L/2}{w_m}\right) - \mathrm{erf}\left(\frac{Y-L/2}{w_m}\right)\right], \tag{21}$$

with $w_m = a + (m-1)b$ and where L is the width of the ion beam along the y axis. Since in practice N is measured for a discrete set of vertical displacements $(Y_1, \ldots, Y_k)$, expansion (16) is written as

$$\mathbf{N} = \mathbf{C}\Psi, \tag{22}$$

where $\mathbf{N}$ is the row vector of data, $\mathbf{C}$ is the row vector of unknown coefficients $(c_1, \ldots, c_{m_{\max}})$, and Ψ is the matrix with elements $\Psi_{ij} = \psi_i(Y_j)$. The problem of finding the coefficients $\mathbf{C}$ in (22) is in general underdetermined as the number $m_{\max}$ of basis functions is larger than the number k of data. An approximate solution to (22) is found by using the non-negative least-square (NNLS) algorithm [29,30]. The NNLS result was further checked using a Tikhonov regularization [31], whose free, smoothing parameter q was chosen at the maximum curvature of the L curve [32]. After the coefficients $\mathbf{C}$ have been found, the expansions of both $N(Y)$ and $p(r)$ are known.

Integrating the photon flux over polar coordinates and over the pulse duration, we obtain

$$2\pi\Delta \int dr\, r\, \phi(r) = \frac{E_{\mathrm{laser}}}{\hbar\omega}. \tag{23}$$

Substituting $\phi(r) = \sqrt{p(r)/\sigma^{(2)}}$ in (23), squaring both members and rearranging, we finally obtain the expression of

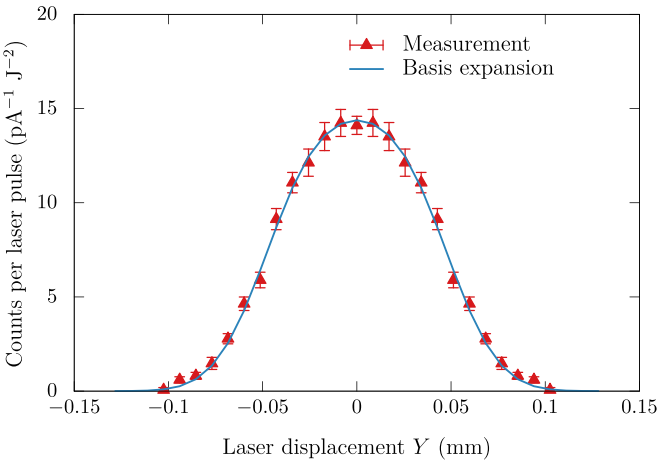

FIG. 3. Number of neutrals per laser pulse (triangles) as a function of the vertical displacement Y of the laser beam. The data are an average over 31 vertical scans. It has been normalized for the laser pulse energy and the ion beam current, and was subsequently symmetrized. The full line is the result obtained from the basis expansion.

the generalized two-photon cross section in terms of known quantities:

$$\sigma^{(2)} = \frac{e\, v}{\eta\, I_{\rm ion}} \left(\frac{\hbar\omega}{E_{\rm laser}}\right)^2 \frac{\Delta^2}{\Delta^{(2)}} \times 4\pi^2 \left[\int dr\, r \sqrt{\sum c_m \varphi_m(r)}\right]^2 . \qquad (24)$$

The measured signal $N(Y)$ is included in this expression through the coefficients c_m. All other factors can be measured precisely, and only reasonable assumptions concerning the ion and laser beams are necessary.

C. Experimental realization

In practice, the laser beam is vertically scanned across the ion beam by tilting a glass plate. At each angle, the laser pulse energy, the ion current, and the yield of neutrals are recorded during 150 laser shots. The scan is repeated several times in order to obtain good statistics.

In Fig. 3, we show an example of the measured detachment yield, normalized for the laser pulse energy and the ion current, and the corresponding expansion on a basis set of 300 Gaussian functions with widths corresponding to laser waists from 30 to 200 μm. We intentionally chose an oversized basis to test the robustness of the method. The NNLS algorithm and the Tikhonov regularization method give the same expansion coefficients to within 2%. They are nonzero only for two functions with widths corresponding to laser waists of 60 and 60.7 μm, in excellent agreement with an independent measurement of the waist. Indeed, by passing a razor blade at the focal point and measuring the transmitted energy as in [15], we estimated the radius of the laser spot to be 60 μm. Using (12), the value obtained for the cross section is $\sigma^{(2)} = 1.49 \times 10^{-49}$ cm^{4}s, while (24) gives $\sigma^{(2)} = 1.50 \times 10^{-49}$ cm^{4}s.

TABLE I. Experimental uncertainties arising from systematic effects.

	One-photon	Two-photon
Vertical displacement Y [15]	2%	2%
Ion velocity v [15]	1%	1%
Power/energy meter $P_{\rm laser}/E_{\rm laser}$	3%	5%
Detection efficiency η	4%	5%
Photodiode rise time		2%
Slit height L		7% to 15%

The uncertainties arising from systematic effects are listed in Table I. The finite response time of the fast photodiode yields an uncertainty in the ratio $\Delta^2/\Delta^{(2)}$, which is estimated to lie below 2%. The energy meter has a 3% calibration accuracy according to the manufacturer, and a comparison with another energy meter gives a 5% uncertainty. The latter thus provides a conservative estimate for the pulse energy error. The uncertainty in the coefficients of the expansion is lower than 3%. The 3% uncertainty in the height L of the slit, which enters the determination of the basis functions Ψ_m in Eq. (21), results in an uncertainty from 7% to 15% in the cross section depending on the quality of the measurement. The total error is then computed following the NIST guidelines [33], and is a simple quadrature sum of the different uncertainties.

IV. THEORY

Cross sections for one- and two-photon detachment of O^- were calculated using the R-matrix Floquet theory, which provides an *ab initio*, nonperturbative description of atomic processes such as multiphoton ionization and laser-assisted electron-atom scattering [16,17,34]. We consider an atomic system comprising $N+1$ electrons in the presence of a homogeneous, linearly polarized laser field of frequency ω, represented in the dipole approximation by the vector potential $A_0\hat{\boldsymbol{\epsilon}} \cos\omega t$. Since the vector potential is periodic, the wave function describing this system can be expanded in a Floquet-Fourier series

$$\Psi(\boldsymbol{X}_{N+1},t) = e^{-iEt} \sum_{n=-\infty}^{\infty} e^{-in\omega t} \Psi_n(\boldsymbol{X}_{N+1}), \qquad (25)$$

where $\boldsymbol{X}_{N+1}$ is the set of space and spin coordinates of all $N+1$ electrons. Substituting (25) into the full time-dependent Schrödinger equation results in an infinite set of time-independent coupled equations for the Floquet components $\Psi_n(\boldsymbol{X}_{N+1})$ which, following the usual R-matrix procedure, are solved in different regions of configuration space using locally adapted bases, gauges, and reference frames.

The R-matrix inner region is bounded by a sphere of radius a chosen to encompass the charge distribution of the N-electron states $\Phi_i(\boldsymbol{X}_N)$ of the residual atom to be taken into account. The Floquet components $\Psi_n(\boldsymbol{X}_{N+1})$ are then expanded in a discrete basis of fully antisymmetrized wave functions built from $\Phi_i(\boldsymbol{X}_N)$ and a set of continuum orbitals $u_j(r)$ for the photoelectron, which satisfy a fixed logarithmic boundary condition at $r = a$. A set of $(N+1)$-electron bound configurations vanishing at $r = a$ is also included to account

for short-range correlation and, more critically in the context of photoionization, to describe the initial bound state of the system. In the inner region, the atom-field interaction is described in the length gauge which is the most appropriate since the radial coordinate of each electron remains smaller than a. Diagonalizing the full $(N+1)$-electron Floquet Hamiltonian yields a set of eigenvalues and eigenvectors that are used to build the R-matrix, defined as the inverse of the matrix of logarithmic derivatives of the reaction channel wave functions, evaluated at the boundary of the inner region.

The outer region of configuration space corresponds to one electron moving beyond the inner region boundary while the other N electrons remain within. The interaction of the field with the bound electrons is still described in the length gauge but its interaction with the ejected electron is now represented in the velocity gauge, which is more appropriate at large distances. Exchange between the ejected and bound electrons is negligible in the outer region so that the equations to be solved reduce to an infinite set of coupled second-order differential equations. These are solved using a close-coupling approach combined with log-derivative propagation up to a sufficiently large distance, where the propagated solutions are matched with a set of asymptotic solutions. These are defined using an asymptotic expansion satisfying Siegert boundary conditions in the acceleration frame. This matching is only possible at particular complex quasienergies $E = \varepsilon - i\Gamma/2$, where ε is the Stark-shifted energy of a dressed state and Γ is its total ionization rate. The quasienergies are found by an iterative search in the complex energy plane. Following lowest-order perturbation theory, the generalized cross section for ionization by n photons is related to the total ionization rate by

$$\sigma^{(n)} = \left(\frac{8\pi\omega\alpha}{I}\right)^n \Gamma, \tag{26}$$

where I is the laser field intensity and α is the fine-structure constant. All quantities in (26) are expressed in atomic units.

It is important to note that the linearly polarized laser field introduces a preferred direction in space and hence breaks its spherical symmetry. As a result, the total angular momentum $\mathcal{L}$ of the full $(N+1)$-electron system is no longer a good quantum number, but its projection $M_\mathcal{L}$ on the polarization axis still is. The generalized cross sections must therefore be calculated for each possible value of $M_\mathcal{L}$ and then averaged in order to compare with experiment. In the case studied here, the initial state of O^- has a $^2P^o$ symmetry and hence $M_\mathcal{L} = 0, \pm 1$. The generalized cross section for two-photon detachment, assuming a statistical distribution of alignments, is then given by

$$\sigma^{(2)} = \tfrac{1}{3}\left(\sigma^{(2)}_{M_\mathcal{L}=0} + 2\sigma^{(2)}_{|M_\mathcal{L}|=1}\right). \tag{27}$$

The first step in our R-matrix Floquet calculations is to define a set of wave functions representing the states of the residual oxygen atom. These are based on configuration interaction (CI) expansions, built from a basis of atomic orbitals. The $(N+1)$-electron R-matrix basis functions, used to describe the initial bound state of O^- as well as the final arrangement channels, are then formed by coupling these atomic states to a set of continuum orbitals representing the photoelectron. The atomic orbitals are also used to define the $(N+1)$-electron bound configurations. The main difficulty is obtaining a reasonable balance in the two CI expansions: increasing the number of residual atomic states included in the calculation, as well as improving their description by increasing the number of configurations in their CI expansion, greatly increases the size of the basis used to represent the negative ion state without necessarily improving its electron affinity. This is illustrated for example in the extensive calculations for the photodetachment of O^- by Zatsarinny and Bartschat [11], where increasing the number of atomic states included in the CI expansion for the initial O^- state first improves but then deteriorates the calculated electron affinity compared to its measured value. Furthermore, since oxygen is an open-shell atom, polarization of the atomic states is expected to play an important role in the photodetachment process. An accurate value for the ground-state static polarizability, for example, in principle requires a large number of atomic bound states as well as a good representation of the continuum which accounts for approximately 75% of the total value. Zatsarinny and Bartschat [11], for example, used a basis expansion involving 108 target states and pseudostates to obtain a polarizability of $4.07\,a_0^3$, compared to the experimental value of $(5.2 \pm 0.4)\,a_0^3$ [35].

In the current experiment, the laser intensity is relatively weak, so that there is little probability of the system absorbing more than two photons. We also consider low photon energies, such that in both the one- and two-photon cases only the $O(1s^2 2s^2 2p^4\ ^3P)$ ground state can be populated. It therefore seems excessive in this case to use a large CI expansion including many target states and pseudostates in order to accurately treat polarization effects. Instead, we use a CI expansion that is voluntarily restricted in order to keep the photoionization calculations simple, yet reproducing with reasonable precision the electron affinity of the $O^-(1s^2 2s^2 2p^5\ ^2P^o)$ initial state as well as the polarizability of the $O(1s^2 2s^2 2p^4\ ^3P)$ ground state. We include the three physical ^3P, ^1D, and ^1S states of oxygen associated with the $1s^2 2s^2 2p^4$ ground configuration, built using the $1s$, $2s$, and $2p$ Hartree-Fock orbitals [37]. We also add the $1s^2 2p^6$ configuration to the ^1S term as this accounts for nearly 4% of the configuration interaction in this state. In order to represent the ground-state polarizability, we add three long-range polarized pseudostates $\overline{^3S^o}$, $\overline{^3P^o}$, and $\overline{^3D^o}$ built using pseudo-orbitals $\bar{3}s$, $\bar{3}p$ and $\bar{3}d$. These pseudo-orbitals are expressed as linear combinations of Slater orbitals whose parameters are determined using a perturbative-variational approach to maximize the ground-state polarizability rather than energies, as implemented in the computer package CIVPOL [38,39]. All configurations involving a single excitation from the $n = 2$ shells are included in the CI expansion for these pseudostates. The polarizability of the $O(1s^2 2s^2 2p^4\ ^3P)$ ground state thus obtained is $5.08\,a_0^3$, well within the error bars on the experimental value of $(5.2 \pm 0.4)\,a_0^3$ [35]. The energies of all six states included in our calculations are given in Table II.

The set of basis functions for the $(N+1)$-electron system includes all configurations built from each of these six atomic states coupled to a continuum orbital $u_{n\ell}$, with $\ell \leqslant 5$ and $n \leqslant 20$, together with all $(N+1)$-electron bound terms generated from one-electron excitations of the two configurations $1s^2 2s^2 2p^5$ and $1s^2 2s 2p^6$. The boundary of the R-matrix inner

TABLE II. Energies in atomic units of the six states and pseudostates of oxygen used in this work. The observed values are taken from the NIST Atomic Spectra Database [36].

	Absolute	Relative	Observed
^{3}P	−74.809 370	0.0	0.0
^{1}D	−74.728 719	0.080 651	0.071 944
^{1}S	−74.662 385	0.146 986	0.153 615
$\overline{^3\text{S}^o}$	−74.226 311	0.583 060	
$\overline{^3\text{D}^o}$	−74.052 693	0.756 677	
$\overline{^3\text{P}^o}$	−73.994 430	0.814 940	

region was taken to be 20 a_0. The electron affinity for the $O^-(1s^2 2s^2 2p^5\ ^2P^o)$ state was determined using the standard suite of *R*-matrix computer programs to be 0.05 380 a.u., while the value obtained in the *R*-matrix Floquet calculations described below is 0.053 799 a.u., in relatively good agreement with the experimental values of 0.053 694 95(7) a.u. and 0.053 695 00(10) a.u. obtained, respectively, by photodetachment microscopy [40] and photodetachment threshold spectroscopy [41]. The experimental value is in fact the electron affinity between the fine-structure ground states of the negative ion and neutral atom. By computing the weighted average of the fine-structure components in the ground multiplets as derived from experiment [40] and the NIST Atomic Spectra Database [36], we find an electron affinity of 0.053 78 a.u., close to the value obtained in the calculations.

We have performed several *R*-matrix Floquet calculations, retaining 1 emission and up to 4 absorption components in the Floquet-Fourier series (25), for various intensities ranging from 10^5 W cm^{-2} up to 2×10^8 W cm^{-2}, in order to verify the convergence and stability of the cross sections. In the case of one-photon detachment, we have also performed a standard *R*-matrix calculation in which the photodetachment process is treated perturbatively in the outer region: the cross section is then related to the dipole matrix element between the initial bound and final continuum state, expressed in either length or velocity form (see, for example, [18] and references therein).

V. RESULTS AND DISCUSSION

A. One-photon detachment

The present results for one-photon detachment are shown in Figs. 4 and 5, along with previous calculations and measurements. Figure 4 compares the *R*-matrix Floquet results with those of the current and four previous experiments [3–6] which were in mutual agreement to within their error bars. Just above threshold, the present measurement is in agreement with that by Lee *et al.* [5]. For photon energies above 2.2 eV, however, it is about 20% larger than the other three experiments, increasing with energy, while the experimental data of [3,4,6] present a plateau with a slightly negative slope.

The measurements by Smith and by Branscomb *et al.* were performed in a crossed-beam configuration. The light from a carbon arc lamp was sent through quasimonochromatic filters onto a beam of O^- and the cross section was inferred by carefully measuring the photoelectron current [1]. This might have been underestimated, however, since the pronounced dip

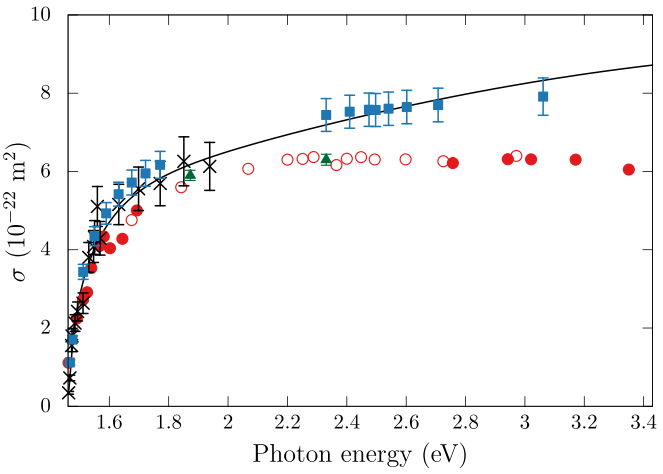

FIG. 4. Experimental cross sections for the one-photon detachment of O^-: open circles, absolute measurement [3]; full circles, relative measurements [4], normalized to the values from [3]; crosses, relative measurement [5] normalized to the D^- cross section; full triangles, absolute measurement [6]; full squares, present measurement. The solid line is the present *R*-matrix Floquet calculation. The error bars are the combined statistical and systematic uncertainties.

in the asymmetry parameter β indicates a major change in the angular distribution of the emitted photoelectrons (see Fig. 6), possibly causing an incomplete collection of the electrons as their energy increases, thereby resulting in a too small cross section.

The recent experiment of Hlavenka *et al.* [6] yields values for the cross section matching those of earlier work. It is based on negative ion depletion in a multipole trap and thus avoids the possible loss of photoelectrons just mentioned. As in this work, the measurement relies on scanning the laser beam across the ion trap in order to avoid having to determine the

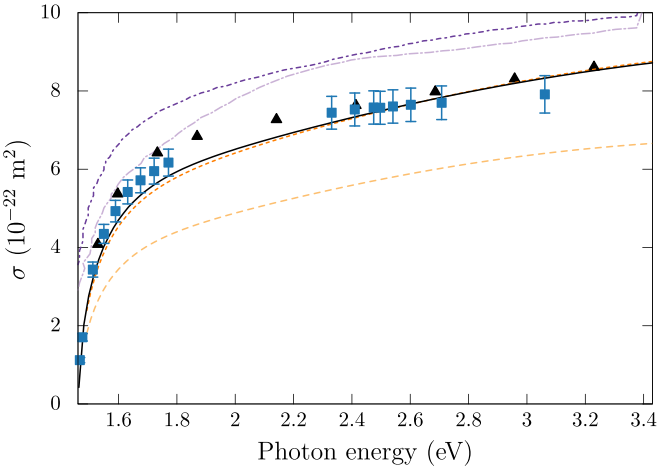

FIG. 5. Theoretical cross sections for the one-photon detachment of O^-: solid line, present *R*-matrix Floquet calculation; dashed and broken lines, present standard *R*-matrix calculation in, respectively, the length and velocity forms; dashed-dotted and chain lines, B-spline *R*-matrix (BSR) results in length and velocity forms [11]; full triangles, perturbation theory using a one-electron model potential [13]. The full squares are the present experiment.

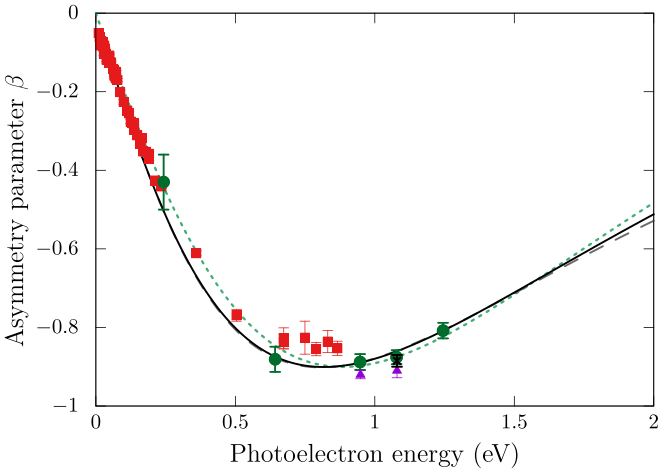

FIG. 6. Asymmetry parameter for the one-photon detachment of $O^-(1s^22s^22p^5\,{}^2P^o)$. The solid and dashed lines are the results obtained from the standard R-matrix calculation using, respectively, the length and velocity forms of the dipole matrix. The full squares [53], full triangles [51], full circles [52], and the cross [50] are experimental values and the dotted line is the formula from Ref. [52].

interaction volume, but the assumptions made concerning the ion density are more stringent. The quoted uncertainty seems rather low, considering the typical accuracy of power meters and the deflection technique employed to scan the trapping volume.

For the sake of completeness, one must mention the early absolute measurements by Branscomb and Smith [1] and later by Branscomb *et al.* [2], performed with a similar experimental setup. These early values were omitted from a subsequent publication by the same authors [4] and are thus not reproduced here. Their magnitudes are lower than those of the present experiment, while their shape is very similar. Several studies [42,43] also measured in great detail the photodetachment signal close to threshold and, by fitting the signal with the Wigner threshold law [44] or using the modified effective range theory of O'Malley *et al.* [45], provided accurate values for the electron affinity of O^- and the spin-orbit splittings between the various fine-structure components of the ground state of the anion and the neutral atom.

Figure 5 compares our experimental results with those of various calculations. There is good agreement between the R-matrix cross sections in length form and those from the R-matrix Floquet method which uses the most appropriate gauge in each region of configuration space. The R-matrix cross sections in velocity form are about 25% smaller. The length and velocity results from a more extensive calculation by Zatsarinny and Bartschat [11], based on the B-spline R-matrix (BSR) method and employing a large number of accurate target states, are in much better mutual agreement, but are approximately 20% larger than those of the R-matrix length and R-matrix Floquet calculations. The early calculation by Robinson and Geltman [13], who used a one-electron model potential adjusted to reproduce the electron affinity, yields results in reasonable agreement with the cross sections from the R-matrix Floquet and R-matrix (length form) calculations. We note that there are a number of other theoretical studies, including semiempirical calculations, whose results are considerably different in both magnitude and shape from those in Figs. 4 and 5 [46–49].

All theoretical results presented here are 20% to 35% larger than the previous experimental data [3–6]. Zatsarinny and Bartschat argued for a systematic error of about 35% in the experimental cross sections of Smith and Branscomb *et al.* [3,4]. Similar values, within experimental error bars, were also obtained by two other independent measurements [5,6]. Moreover, the shapes of the curves of the measured and calculated cross section do not match. Above 2.2 eV, the experimental data are nearly constant with photon energy while the theoretical values increase monotonically. The present measurement is in agreement with the present calculation and that by Robinson and Geltman [13], as both lie within the experimental uncertainty. It is, however, about 15% lower than the calculation by Zatsarinny and Bartschat [11]. The shape of the experimental cross section deviates from the R-matrix Floquet and R-matrix calculations by a steeper rise just above threshold and a more gentle slope at higher energy.

In Fig. 6, we compare the asymmetry parameter β obtained from our standard R-matrix calculation with experimental data [50–53] and the formula of Hanstorp *et al.* [52]. The length and velocity forms of the R-matrix calculation are very similar for photoelectron energies from threshold to just below 1.6 eV, and are in very good agreement with the measured values. Differences between the length and velocity forms become more apparent at higher photoelectron energies. These results thus demonstrate that our restricted CI description is capable of reproducing reasonably well the one-photon detachment process, despite the fact that we use essentially only Hartree-Fock wave functions for the three physical atomic states. This gives us further confidence in the model when turning to the two-photon detachment process.

B. Two-photon detachment

Our results for the two-photon detachment of $O^-(1s^22s^22p^5\,{}^2P^o)$ are shown in Fig. 7. The dotted-dashed, broken, and full curves correspond, respectively, to the R-matrix Floquet results for $M_{\mathcal{L}} = 0$, $|M_{\mathcal{L}}| = 1$ and their statistically averaged sum (27). The parameters of the R-matrix Floquet calculations are the same as for one-photon detachment. We have verified that the generalized cross sections remain stable with increasing laser intensity up to 10^{10} W cm^{-2}. The averaged sum displays a maximum for a photon energy in the region of 0.95 eV, corresponding to a photoelectron energy of about 0.234 eV, coming mainly from the $|M_{\mathcal{L}}| = 1$ contribution which is dominant over most of the energies considered here. The results of the perturbation theory calculation by Robinson and Geltman [13] also display a similar maximum albeit some 10% larger than in the R-matrix Floquet case. The results of Gribakin and Kuchiev [14,54] are about twice those of the R-matrix Floquet calculation. They were obtained from an analytical formula for the n-photon detachment cross sections ($n \geqslant 2$) of negative ions, derived from an adiabatic-theory approach. This expression should give better results when more photons are absorbed. At the photon energy of 1.165 eV, corresponding to a Nd:YAG laser, the R-matrix Floquet calculations yield a

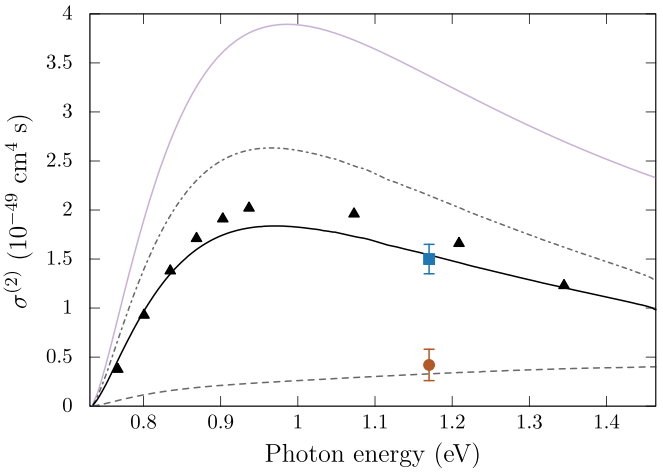

FIG. 7. Generalized cross section for two-photon detachment of $O^-(1s^22s^22p^5\,{}^2P^o)$. The dotted-dashed and broken lines are the present R-matrix Floquet results for $M_\mathcal{L} = 0$ and $M_\mathcal{L} = 1$, respectively, while the solid line is their statistical average (27). The full triangles are the results from perturbation theory based on a one-electron model potential [13]. The thin solid line is the result obtained from the adiabatic-theory approach [14]. The full circle is the experimental value of [12] while the full square is our absolute experimental result. The error bars are the combined statistical and systematic uncertainties.

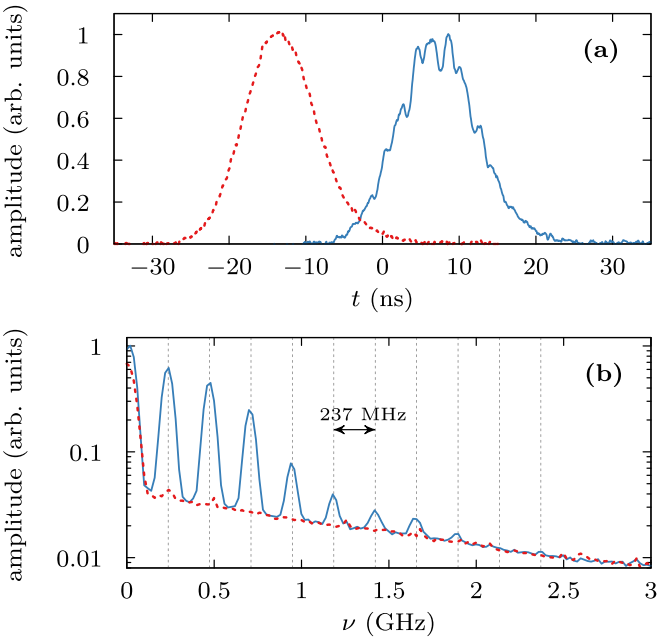

FIG. 8. (a) Temporal profile of the pulses from the seeded (dashed) and unseeded (full) Nd:YAG laser, and (b) norm of the Fourier transform of the difference between the temporal profile of a single pulse and the mean temporal profile, averaged over 500 pulses. The temporal profile of the seeded laser has been shifted in time for clarity. The vertical dashed lines indicate integer multiples of the free spectral range of the laser cavity.

generalized cross section of 1.55×10^{-49} cm^4 s, some 20% smaller than that obtained using perturbation theory [13] and thus much larger than the older experimental value [12]. Our new measurement gives a generalized cross section of $(1.50 \pm 0.16) \times 10^{-49}$ cm^4 s, almost four times larger than the previous experiment and thus in very good agreement with the results of our R-matrix Floquet calculations and those obtained by Robinson and Geltman [13].

Let us now consider the influence of the photon statistics on the experimental generalized cross section. It is well established that temporal fluctuations of the intensity due to mode beating enhance the efficiency of n-photon ionization and detachment [19–21]. In the limit of an infinite number of modes, the enhancement factor reaches $n!$. Pulsed, high-power lasers exhibit in general a large number of modes and previous studies of two-photon detachment have taken the photon statistics into account by dividing the value of the cross section extracted from the data by two [12]. Our Nd:YAG laser also operates in the multimode regime, but can be seeded to force single-mode operation. It is possible to characterize the distribution of the modes by measuring the temporal profile of the laser pulses. Figure 8(a) shows such profiles measured with a 25-GHz photodiode connected to a 3-GHz oscilloscope, with the full line corresponding to the unseeded case and the dashed line to the seeded one. Figure 8(b) shows the norm of the Fourier transform of the difference between the temporal envelope of a single pulse and the mean temporal envelope, averaged over 500 pulses. In the seeded case, the temporal envelope is smooth, as expected for single-mode operation, and, in the Fourier spectrum, the single peak centered at the origin is reminiscent of the Fourier transform of the envelope. In the multimode case (full line), intensity modulations due to mode beating appear on the temporal profile and, in the Fourier spectrum, eight additional peaks are observed at integer multiples of the 237-MHz frequency, which matches the free spectral range of the cavity. The laser pulse therefore consists of at least nine modes.

The generalized cross section extracted from the data is $(1.59 \pm 0.27) \times 10^{-49}$ cm^4 s in the multimode case and $(1.50 \pm 0.16) \times 10^{-49}$ cm^4 s in the single-mode case, therefore, surprisingly, no effect of photon statistics is observed within the error bars. The possible reasons for such an absence are twofold. First, the number of modes is low, hence, deviations due to photon statistics may be lower than $n!$. As an example, the experiment of Lecompte *et al.* [20] considered the 11-photon ionization of xenon for an increasing number of modes and approximately reached the $n!$ factor when more than 100 modes were present in the cavity. Second, in the present crossed-beam configuration, the traversal time of the anions through the diameter of the square of the spatial intensity profile is about 273 ps while the intensity modulations due to mode beating have a period higher than ∼1 ns. As the ions travel through the laser spot, the pulse envelope is essentially constant, and photon statistics do not influence the two-photon detachment process.

VI. CONCLUSIONS

We have reported on the joint theoretical and experimental determination of photodetachment cross sections of the oxygen anion. The one-photon cross section was measured using the animated-crossed-beam technique and is

significantly larger than those from previous experiments. This has important implications since the O^- photodetachment cross section has often been used to normalize relative cross sections for other negative ions. The theoretical calculations based on R-matrix Floquet and standard R-matrix theory used relatively simple representations of the atomic and ionic states. Despite their apparent simplicity, these wave functions reproduce very well the electron affinity of oxygen and the polarizability of its ground state. The results obtained are in much better agreement with the present experiment than another more extensive calculations [11] with better thresholds but less accurate values for the affinity and polarizability.

The generalized two-photon detachment cross section was determined using R-matrix Floquet theory with the same atomic wave functions. The absolute measurement was performed with an extension of the animated crossed-beam technique, based on the deconvolution and Abel inversion of the detachment signal through a basis expansion. The experimental result, at the Nd:YAG wavelength (1604 nm), is in good agreement with the R-matrix Floquet calculation, thus resolving another long-standing discrepancy.

Extending the range of wavelengths studied, both for one- and two-photon processes, is a perspective for future work. Of particular interest is the opening of the $O(^1D)$ one-photon detachment threshold for photon energies above 3.43 eV. The photodetachment of other negative ions can also be considered. Although extensive calculations exist for one-photon detachment, theoretical data are much scarcer for multiphoton detachment of, for example, C^-. Experimental data are also limited, often to just the Nd:YAG and Ar^+ laser wavelengths. The basis expansion method is readily applicable to higher-order processes, e.g.,, the three-photon detachment of F^-. Finally, the animated-crossed-beam technique is not restricted to photodetachment, but can also be applied to photoionization and photodissociation. These will be considered in future work.

ACKNOWLEDGMENTS

The authors thank C. Blondel, G. Gribakin, and R. Wester for fruitful discussions, and S. Gibson for providing us with the numerical values of the measured asymmetry parameter. This work was supported by the Fonds de la Recherche Scientifique–FNRS through IISN Contract No. 4.4504.10. Calculations were performed on the cluster at the Institute of Physics of Rennes.

APPENDIX: PULSED ION BEAMS

In the main part of the paper, we considered the case of a continuous ion beam. However, *pulsed* ion beams are also frequent, e.g., when using a pulsed supersonic expansion or when buffer-gas cooling is applied prior to the interaction with the laser beam. This appendix shows how the ACBT equations can be modified in order to account for such situations.

The two pulsed beams yield two time coordinates for the ions: (i) the coordinate t, relative to the beginning of the ion burst; (ii) the coordinate τ, relative to the center of the laser pulse envelope. The delay T between the beginning of the ion burst ($t = 0$) and the center of the laser pulse envelope ($\tau = 0$) is an experimental parameter and in principle can be adjusted at will. The coordinates t and τ are related through $\tau = t - T$.

The yield $N(Y,T)$ of neutrals now depends on the delay T and Eq. (5) must be modified accordingly:

$$N(Y,T) = \frac{\eta\sigma^{(n)}}{\mathrm{e}\,v}\int dt \iint_S dy\,dz\; j(y,z,t) \times \int_{-\infty}^{+\infty} dx\;\Phi^n\left(x,y-Y,z,t-T+\frac{x}{v}\right). \quad \text{(A1)}$$

By integrating both sides of (A1) over Y and T, we obtain an expression similar to (6):

$$\sigma^{(n)} = \frac{\mathrm{e}\,v}{\eta}\left[\iint dY\,dT\;N(Y,T)\right]\left[\int dt \iint_S dy\,dz\; j(y,z,t) \times \iiint_{-\infty}^{+\infty} dT\,dY\,dx\;\Phi^n\left(x,y-Y,z,t-T+\frac{x}{v}\right)\right]^{-1}. \quad \text{(A2)}$$

For one-photon processes ($n = 1$), the integral of the photon flux Φ over T, Y, and x reduces to the number of photons per pulse $E_{\mathrm{laser}}/\hbar\omega$. The integral of the current density j over t, y, and z is the number of ions per pulse multiplied by the elementary charge $\mathrm{e}N_{\mathrm{ion}}$. Therefore, Eq. (A2) becomes

$$\sigma^{(1)} = \frac{v}{\eta}\left[\iint dT\,dY\;N(Y,T)\right]\frac{\hbar\omega}{N_{\mathrm{ion}}E_{\mathrm{laser}}}. \quad \text{(A3)}$$

For multiphoton processes ($n \geqslant 2$), and under the same assumptions as in Sec. III A, an equation analogous to (10) can be obtained from (A2):

$$\int dT\;N(Y,T) = \frac{\eta\sigma^{(n)}}{v}\Delta^{(n)}N_{\mathrm{ion}}\int dy\;\rho_y(y) \times \int_{-\infty}^{\infty} dx\;\phi^n(x,y-Y). \quad \text{(A4)}$$

Procedures identical to those of Sec. III B can then be used to obtain an expression for the generalized n-photon detachment cross section in terms of precisely measurable quantities. The ACBT can therefore accommodate the use of pulsed ion beams at the expense of an additional scan of the delay between the ion and laser pulses.

[1] L. M. Branscomb and S. J. Smith, Phys. Rev. **98**, 1028 (1955).

[2] L. M. Branscomb, D. S. Burch, S. J. Smith, and S. Geltman, Phys. Rev. **111**, 504 (1958).

[3] S. J. Smith, in *Proceedings of the Fourth International Conference on Ionization Phenomena in Gases, Uppsala, 17–21 August 1959*, edited by N. Robert Nilsson (North-Holland Publishing Company, Amsterdam, 1960), Vol. 1, p. IC-219.

[4] L. M. Branscomb, S. J. Smith, and G. Tisone, J. Chem. Phys. **43**, 2906 (1965).
[5] L. C. Lee and G. P. Smith, J. Chem. Phys. **70**, 1727 (1979).
[6] P. Hlavenka, R. Otto, S. Trippel, J. Mikosch, M. Weidemüller, and R. Wester, J. Chem. Phys. **130**, 061105 (2009).
[7] M. L. Seman and L. M. Branscomb, Phys. Rev. **125**, 1602 (1962).
[8] G. Haeffler, D. Hanstorp, I. Y. Kiyan, U. Ljungblad, H. H. Andersen, and T. Andersen, J. Phys. B: At., Mol. Opt. Phys. **29**, 3017 (1996).
[9] P. Kristensen, H. H. Andersen, P. Balling, L. D. Steele, and T. Andersen, Phys. Rev. A **52**, 2847 (1995).
[10] D. S. Burch, S. J. Smith, and L. M. Branscomb, Phys. Rev **112**, 171 (1958).
[11] O. Zatsarinny and K. Bartschat, Phys. Rev. A **73**, 022714 (2006).
[12] H. Stapelfeldt, C. Brink, and H. K. Haugen, J. Phys. B: At., Mol. Opt. Phys. **24**, L437 (1991).
[13] E. J. Robinson and S. Geltman, Phys. Rev. **153**, 4 (1967).
[14] G. F. Gribakin and M. Y. Kuchiev, Phys. Rev. A **55**, 3760 (1997).
[15] M. Génévriez and X. Urbain, Phys. Rev. A **91**, 033403 (2015).
[16] P. G. Burke, P. Francken, and C. J. Joachain, J. Phys. B: At., Mol. Opt. Phys. **24**, 761 (1991).
[17] M. Dörr, M. Terao-Dunseath, J. Purvis, C. J. Noble, P. G. Burke, and C. J. Joachain, J. Phys. B: At., Mol. Opt. Phys. **25**, 2809 (1992).
[18] P. G. Burke, *R-Matrix Theory of Atomic Collisions*, Springer Series on Atomic, Optical, and Plasma Physics, Vol. 61 (Springer, Berlin, 2011).
[19] P. Lambropoulos, Adv. At. Mol. Phys. **12**, 87 (1976).
[20] C. Lecompte, G. Mainfray, C. Manus, and F. Sanchez, Phys. Rev. A **11**, 1009 (1975).
[21] L. Mandel and E. Wolf, Rev. Mod. Phys. **37**, 231 (1965).
[22] A. Naji, K. Olamba, J. P. Chenu, S. Szücs, M. Chibisov, and F. Brouillard, J. Phys. B: At., Mol. Opt. Phys. **31**, 2961 (1998).
[23] F. Brouillard and P. Defrance, Phys. Scr. **T3**, 68 (1983).
[24] P. Defrance, F. Brouillard, W. Claeys, and G. Van Wassenhove, J. Phys. B: At., Mol. Phys. **14**, 103 (1981).
[25] J. J. Blangé, X. Urbain, H. Rudolph, H. A. Dijkerman, H. C. W. Beijerinck, and H. G. M. Heideman, J. Phys. B: At., Mol. Opt. Phys. **29**, 2763 (1996).
[26] R. N. Bracewell, *The Fourier Transform and Its Applications*, 3rd ed. (McGraw Hill, Boston, 2000).
[27] R. D. Guenther, *Modern Optics* (Wiley, New York, 1990).
[28] B. J. Whitaker, *Imaging in Molecular Dynamics: Technology and Applications* (Cambridge University Press, Cambridge, 2003).
[29] C. L. Lawson and R. J. Hanson, *Solving Least Squares Problems* (SIAM, Philadelphia, 1995), p. 351.
[30] E. Jones, T. Oliphant, P. Peterson *et al.*, SciPy: Open source scientific tools for PYTHON, http://www.scipy.org/ (2001).
[31] A. N. Tikhonov and V. Y. Arsenin, *Solutions of Ill-posed Problems* (Wiley, New York, 1977).
[32] P. C. Hansen, SIAM Rev. **34**, 561 (1992).
[33] B. N. Taylor and C. N. Kuyatt, NIST Tech. Note No. 1297, 1994.
[34] M. Terao-Dunseath and K. M. Dunseath, J. Phys. B: At., Mol. Opt. Phys. **35**, 125 (2002).
[35] R. A. Alpher and D. R. White, Phys. Fluids **2**, 153 (1959).
[36] NIST Atomic Spectra Database, http://www.nist.gov/pml/data/asd.cfm.
[37] E. Clementi and C. Roetti, At. Data Nucl. Data Tables **14**, 177 (1974).
[38] V. K. Lan, M. Le Dourneuf, and P. G. Burke, J. Phys. B: At. Mol. Phys. **9**, 1065 (1976).
[39] M. Le Dourneuf, *Traitement unifié des états liés et des états collisionnels des systèmes atomiques complexes par la méthode du coeur gelé polarisé*, Ph.D. thesis, Université Pierre et Marie Curie, 1976.
[40] C. Blondel, C. Delsart, C. Valli, S. Yiou, M. R. Godefroid, and S. Van Eck, Phys. Rev. A **64**, 052504 (2001).
[41] D. M. Pendergrast and J. N. Yukich, Phys. Rev. A **67**, 062721 (2003).
[42] D. M. Neumark, K. R. Lykke, T. Andersen, and W. C. Lineberger, Phys. Rev. A **32**, 1890 (1985).
[43] T. Suzuki and T. Kasuya, Phys. Rev. A **36**, 2129 (1987).
[44] E. P. Wigner, Phys. Rev. **73**, 1002 (1948).
[45] T. F. O'Malley, L. Spruch, and L. Rosenberg, J. Math. Phys. **2**, 491 (1961).
[46] C. M. Oana and A. I. Krylov, J. Chem. Phys. **131**, 124114 (2009).
[47] G. Miecznik and C. H. Greene, Phys. Rev. A **53**, 3247 (1996).
[48] R. L. Chase and H. P. Kelly, Phys. Rev. A **6**, 2150 (1972).
[49] R. J. W. Henry, Phys. Rev. **162**, 56 (1967).
[50] J. L. Hall and M. W. Siegel, J. Chem. Phys. **48**, 943 (1968).
[51] F. Breyer, P. Frey, and H. Hotop, Z. Phys. A: At. Nucl. **286**, 133 (1978).
[52] D. Hanstorp, C. Bengtsson, and D. J. Larson, Phys. Rev. A **40**, 670 (1989).
[53] S. J. Cavanagh, S. T. Gibson, and B. R. Lewis, J. Phys. Conf. Ser. **212**, 012034 (2010).
[54] G. F. Gribakin and M. Y. Kuchiev, J. Phys. B: At., Mol. Opt. Phys. **30**, L657 (1997).